VI International Conference on Computational Methods in Marine Engineering
MARINE 2015
F. Salvatore, R. Broglia and R. Muscari (Eds)

NUMERICAL STUDIES FOR VERIFICATION AND VALIDATION OF OPEN-WATER PROPELLER RANS COMPUTATIONS

JOÃO M. BALTAZAR*, DOUWE R. RIJPKEMA† AND JOSÉ A. FALCÃO DE CAMPOS§

*Instituto Superior Técnico (IST)
Universidade de Lisboa, Av. Rovisco Pais 1, 1049-001 Lisboa, Portugal
e-mail: joao.baltazar@tecnico.ulisboa.pt, web page: http://tecnico.ulisboa.pt/

†Maritime Research Institute Netherlands (MARIN)
2, Haagsteeg, 6708 PM Wageningen, the Netherlands
e-mail: d.r.rijpkema@marin.nl - Web page: http://www.marin.nl

§Instituto Superior Técnico (IST)
Universidade de Lisboa, Av. Rovisco Pais 1, 1049-001 Lisboa, Portugal
e-mail: falcao.campos@tecnico.ulisboa.pt, web page: http://tecnico.ulisboa.pt/

Key words: Marine Propellers, Open-Water, RANS, Verification and Validation

Abstract. In this paper, viscous flow calculation using a RANS method are presented for two marine propellers in open-water conditions at model-scale. A verification study from a range of geometrically similar grids with different grid densities is made. The results show that the numerical uncertainties for the propeller forces are in the order of 0.4%-2.2%. The influence of the domain size and boundary conditions on the prediction of the propeller forces is analysed. The numerical predictions are compared with the experimental results. These differences (comparison error) are larger than the numerical uncertainty, suggesting that the comparison error is dominated by the modelling error.

1 INTRODUCTION

The physical flow features around propellers operating behind a ship hull can vary significantly depending on the geometry of the propeller and its loading. Capturing these flow features using a viscous CFD (Computational Fluid Dynamics) method, for example RANS (Reynolds-Averaged Navier-Stokes) method, requires detailed knowledge on the influence of the grid topology, domain size, turbulence model, Reynolds number, etc. However, some of these flow features may not be relevant if one is only interested in the shaft forces and moments, while the fine grids that are required to capture all flow features

will lead to very excessive CPU time. It is therefore necessary to have a good working knowledge on how to analyse propellers with a CFD method in a cost-effective way for both model-scale and full-scale conditions.

This knowledge can be improved by analysing a wide range of propeller geometries in open-water condition using numerical uncertainty analysis [1] for a series of grids to quantify the different sources of errors. A verification and validation study for different marine propulsors can be found in [2].

In this paper, viscous flow calculations using a CFD method are presented for two marine propellers in open-water conditions at model-scale. First, a numerical uncertainty analysis from a range of geometrically similar grids with different grid densities is made. The influence of the domain size and boundary conditions on the numerical predictions is considered next. Finally, the force coefficients are compared with experimental data available from open-water tests. The paper is organised as follows: a description of the numerical tool is given in the next section; the verification and validation procedures are presented in Section 3; in Section 4 the test-cases and the numerical set-up are considered; the model-scale performance prediction of both propellers is treated in Section 5; the paper ends with the conclusions of the present study.

2 RANS CODE REFRESCO

ReFRESCO is a MARIN in-house viscous flow CFD code [3]. It solves the multiphase (unsteady) incompressible RANS equations, complemented with turbulence models, cavitation models and volume fraction transport equations for different phases. The equations are discretised using a finite-volume approach with cell-centred collocation variables. A strong-conservation form and a pressure-correction equation based on the SIMPLE algorithm is used to ensure mass conservation. The implementation is face-based, which permits grids with elements consisting of an arbitrary number of faces (hexahedrals, tetrahedrals, prisms, pyramids, etc.), and h-refinement (hanging nodes). The code is parallelised using MPI and sub-domain decomposition, and runs on Linux workstations and HPC clusters. For turbulence modelling, RANS/URANS, SAS and DES approaches can be used. ReFRESCO is currently being developed within a cooperation led by MARIN.

For a marine propeller in uniform inflow conditions the equations can be solved using a so-called absolute formulation. This means that the velocity vector $\vec{V}$ is defined in the absolute or inertial earth-fixed reference frame, with the equations being solved in the body-fixed reference frame which is rotating with velocity Ω. This allows to perform steady simulations for open-water conditions. For all the calculations presented in this paper, the $\kappa - \omega$ SST 2-equation eddy-viscosity model proposed by Menter [4] is used. A second-order convection scheme (QUICK) is used for the momentum equations and a first-order upwind scheme is used for the turbulence model.

3 VERIFICATION AND VALIDATION PROCEDURES

The use of any numerical method calls for an analysis of the numerical errors involved. For CFD methods there are three different contributions to the numerical error: round-off error as a consequence of the finite precision of the computers, iterative error related to the non-linearity of the transport equations, and discretisation error due to the discrete representation (in space and time) of a (partial) differential equation. While round-off errors can be considered to be low, the iterative and discretisation errors are more difficult to control. The iterative errors are commonly monitored with the variation of the residuals during the simulation and should be several orders of magnitude lower than the discretisation error, in order to perform a correct verification study. The discretisation error can only be determined for cases that have an exact solution, but for more complex cases without exact solution an estimate can be obtained by performing a numerical uncertainty analysis, commonly referred to as verification. The goal of verification is to estimate the uncertainty of a given numerical prediction U_{num}, i.e. an interval that contains the exact solution with 95% confidence,

$$\phi_i - U_{\text{num}} \leq \phi_{\text{exact}} \leq \phi_i + U_{\text{num}}. \tag{1}$$

In this study the numerical uncertainty is determined following the procedure described in [1]. The numerical uncertainty is determined using

$$U_{\text{num}} = F_s|\epsilon|, \tag{2}$$

where F_s represents a safety factor and ϵ denotes an estimate of the discretisation error. The discretisation error is estimated by

$$\epsilon = \phi_i - \phi_0 = \alpha h_i^p, \tag{3}$$

in which ϕ_i stands for any integral or local flow quantity, ϕ_0 is the estimate of the exact solution, α a constant, p is the observed order of accuracy and h_i is the typical cell size of grid i, determined in our case from the total number of grid cells N_{cells} by $h_i = (1/N_{\text{cells}})^{1/3}$. The estimation of ϵ requires the determination of ϕ_0, α and p. The unknown coefficients in Equation (3) are determined from a least-square fit of the numerical solutions on geometrically similar grids with different densities. The error estimation is considered reliable if the apparent order is within the expected order of discretisation. In this case, a low safety factor of $F_s = 1.25$ is applied, otherwise $F_s = 3$. The complete procedure is described in [1].

The goal of validation is to quantify the modelling uncertainty, i.e. to quantify how well the mathematical model represents the physical world. The difference between the numerical and experimental results, referred to as the comparison error E, can be subsequently be compared to the total validation uncertainty U_{val}, which includes the experimental uncertainty in addition to the numerical uncertainties. If the comparison error is within the validation uncertainty and the validation uncertainty is sufficiently small, the results

can be said to be validated within that uncertainty. If the comparison error is larger than the validation uncertainty, the comparison error is probably dominated by the modelling error, which indicates that the model must be improved.

4 MODEL GEOMETRY AND GRID GENERATION

Two propellers, designated S6368 and S6408, are considered in the present study. Their particulars are listed in Table 1, where D is the propeller diameter, $c_{0.7R}$ the blade chord length at 0.7 of the propeller radius R, Z the number of blades, $P/D_{0.7R}$ the pitch-diameter ratio at $0.7R$ and A_E/A_0 the blade-area ratio. The propeller S6408 has a relatively simple geometry with almost no skew and no rake. The propeller S6368 has a lower blade-area ratio and a larger skew. A set of experiments for the two propellers have been carried out in the depressurised towing tank of MARIN.

Table 1: Overview of propeller particulars.

	S6368	S6408
D [m]	0.2714	0.3010
$c_{0.7R}$ [m]	0.0694	0.0794
Z	4	4
$P/D_{0.7R}$	0.757	0.711
A_E/A_0	0.456	0.481

Table 2: Overview of the grid sizes and number of cell faces on a single blade. The corresponding maximum y^+ values are for the design condition at model scale.

	S6368			S6408		
	Volume	Blade	y^+	Volume	Blade	y^+
G1	34.8M	39K	0.34	41.3M	51K	0.27
G2	17.8M	25K	0.42	23.7M	35K	0.37
G3	8.0M	15K	0.52	11.3M	21K	0.32
G4	4.3M	10K	0.62	6.9M	15K	0.40
G5	2.2M	6K	0.78	2.3M	7K	0.59
G6	1.0M	2K	0.95	1.0M	4K	0.63

For the two propeller geometries six geometrically similar structured grids have been generated. The grids range from 1 to 35 million cells and from 1 to 41 million cells for the propellers S6368 and S6408 respectively. In Table 2 the number of cells in the volume and on a single blade are listed for each propeller. The near wall resolution is chosen such that the boundary layer is fully resolved and no wall functions are required. A fine

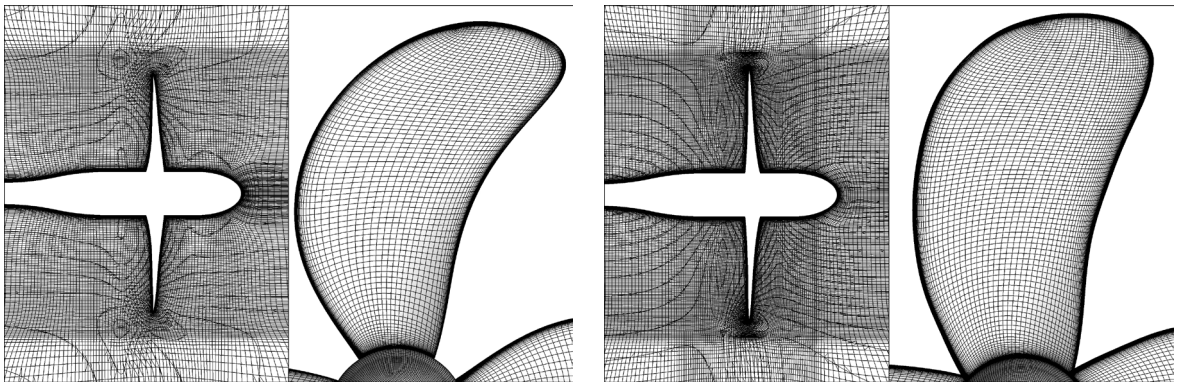

Figure 1: Overview of the grids around propeller and on propeller blades. Grids with 8 million cells for the S6368 (left) and with 11 million cells for the S6408 (right).

boundary layer resolution is obtained, where the maximum y^+ is lower than 1 for all grids. An overview of the grids with 8 million cells for the S6368 and with 11 million cells for the S6408 are presented in Figure 1. A higher density of cells is visible in the propeller region. On the blade surface a higher level of refinement is seen near the propeller edges due to the local curvature.

Unless stated otherwise a cylindrical domain is considered, where the inlet, the outlet and the outer boundary are located 5 propeller diameters from the propeller reference plane. The boundary conditions are the following: at the outer boundary a constant pressure is set; at the inlet a uniform velocity and a low turbulence level are prescribed; at the outlet an outflow condition of zero downstream gradient is used. On the propeller blades and shaft a non-slip condition is used.

5 RESULTS

5.1 General

The viscous flow calculations are carried out in open-water conditions. The propeller operation conditions are defined by the advance coefficient $J = U/(nD)$, where U is the propeller advance speed and $n = \Omega/(2\pi)$ the rotation rate. The open-water characteristics are expressed in the thrust coefficient K_T, the torque coefficient K_Q and the open-water efficiency η_0, defined as follows:

$$K_T = \frac{T}{\rho n^2 D^4}, \quad K_Q = \frac{Q}{\rho n^2 D^5}, \quad \eta_0 = \frac{J}{2\pi}\frac{K_T}{K_Q}, \tag{4}$$

where T is the propeller thrust, Q the propeller torque and ρ the fluid density.

The propeller S6368 is calculated for a range of advance coefficients between 0.1 and 0.8, corresponding to Reynolds numbers from 5.3×10^5 to 5.6×10^5. The propeller S6408 is calculated for a range of advance coefficients between 0.1 and 0.75, corresponding to Reynolds numbers from 7.0×10^5 to 7.4×10^5. The Reynolds number is defined based on the propeller blade chord length at $0.7R$ and the resulting onset velocity at that radius:

$$Re = \frac{c_{0.7R}\sqrt{U^2 + (n\pi 0.7D)^2}}{\nu}, \tag{5}$$

where ν is the fluid kinematic viscosity.

For the S6368 propeller, the initial and inflow turbulence quantities are set to 2% turbulence intensity and an eddy viscosity ratio of 5. For the S6408 propeller, the turbulent intensity and the eddy viscosity ratio are set to 1% and 1, respectively.

5.2 Numerical errors

In this section an analysis of the iterative error and the discretisation error of the computations is performed. In this study, the iterative error is analysed from the infinity norm L_∞ and L_2 norm of the normalised residuals

$$\begin{aligned} L_\infty(\phi) &= \max|\mathrm{res}(\phi_i)|, \quad 1 \le i \le N_{\mathrm{cells}}, \\ L_2(\phi) &= \sqrt{\sum_{i=1}^{N_{\mathrm{cells}}} \mathrm{res}^2(\phi_i) \Big/ N_{\mathrm{cells}}} \end{aligned} \tag{6}$$

Results are presented for grid G3. The iterative convergence of the L_∞ and L_2 norms for the Cartesian components of the flow velocity $V_{x,y,z}$, pressure p and turbulent quantities κ and ω is plotted in Figure 2 for both propellers at a high loading condition. Figure 2 also presents the variation of the thrust and torque coefficients with the number of iterations. Iterative convergence of the flow quantities is difficult to obtain. Convergence of the infinity norm for the velocity residuals is seen between 10^{-2} and 10^{-3}. For the pressure iterative convergence of the L_∞ is achieved to at least one order lower, and for the turbulent quantities the maximum residuals are lower than 10^{-5}. For both propellers the maximum velocity residuals are obtained near the blade tip, where flow separation is seen from the limiting streamlines on the suction side of the blades (see [5]). For the S6368 propeller, trailing edge separation is observed on the suction side at the inner radii [5]. Despite the fact that large residuals are obtained locally for the flow velocity components, iterative convergence of the L_2 norm is obtained to 10^{-5}. For the propeller forces convergence is achieved after 1500 iterations, when the L_∞ and L_2 norms of the flow quantities are not yet converged. From these results, a small effect of the iterative error is expected on the propeller force coefficients.

To estimate the discretisation error six geometrically similar structured grids have been generated. The variation of the thrust, torque and open-water efficiency for each grid compared to the finest grid is listed in Table 3 for both propellers at a highly loading condition and near design condition. A reduction in the variation of the open-water quantities with the increase of the number of cells is obtained. Differences lower than 1% are achieved for grid G3. The results of the numerical uncertainty analysis are plotted in

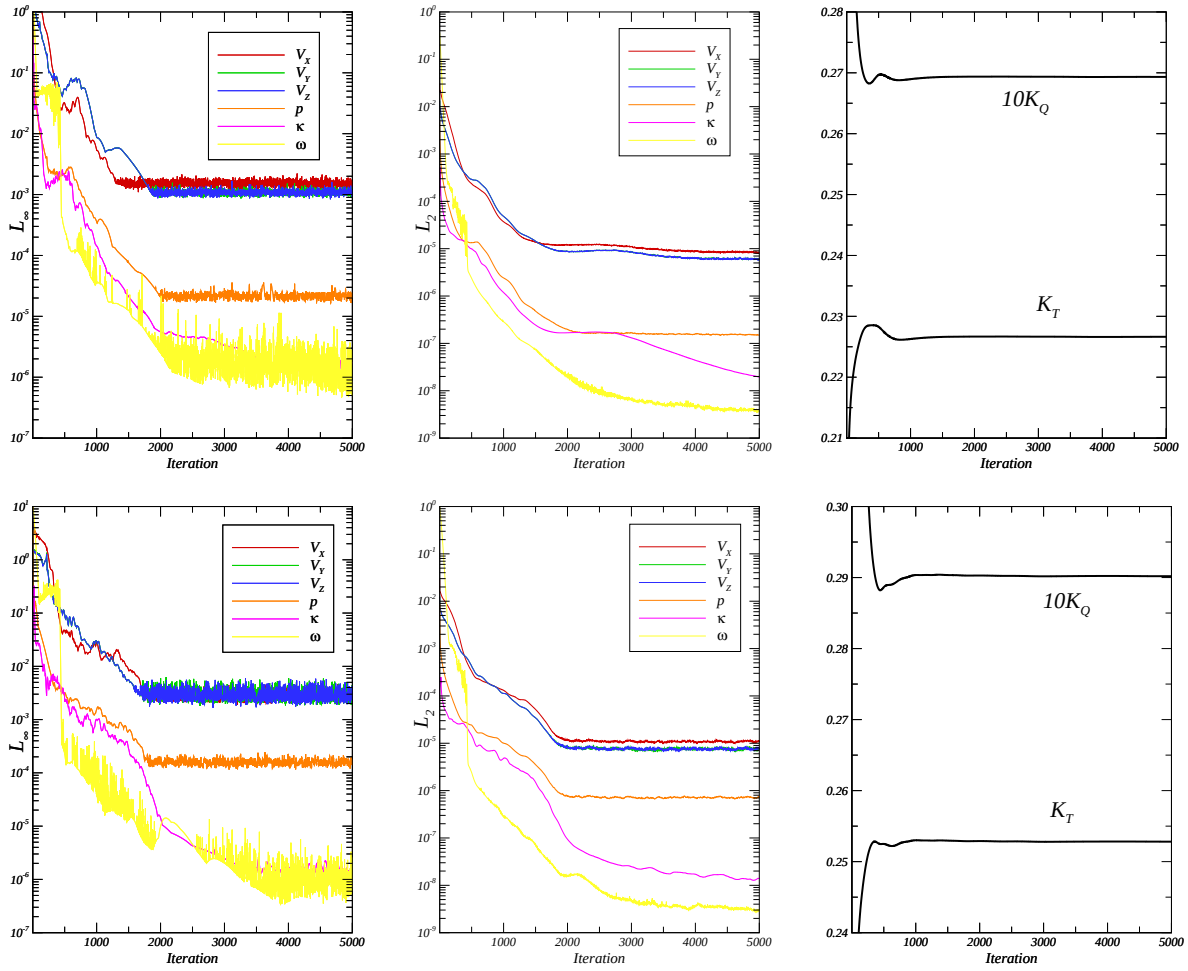

Figure 2: L_∞ (left) and L_2 (middle) iterative convergence and variation of forces (right) for propeller S6368 at $J = 0.3$ (top) and for propeller S6408 at $J = 0.2$ (bottom).

Table 3: Variation of the force coefficients with grid density compared to the finest grid for propellers S6368 and S6408.

	S6368						S6408					
J	0.30			0.65			0.2			0.5		
Grid	ΔK_T	ΔK_Q	$\Delta\eta_0$	ΔK_T	ΔK_Q	$\Delta\eta_0$	ΔK_T	ΔK_Q	$\Delta\eta_0$	ΔK_T	ΔK_Q	$\Delta\eta_0$
G6	1.5%	3.1%	-1.5%	3.9%	5.8%	-1.8%	0.6%	2.0%	-1.4%	2.8%	3.9%	-1.0%
G5	1.0%	1.6%	-0.5%	2.0%	2.6%	-0.6%	0.6%	1.1%	-0.7%	1.8%	2.2%	-0.3%
G4	0.5%	0.8%	-0.2%	1.0%	1.4%	-0.5%	0.4%	0.4%	-0.4%	0.9%	0.9%	0.0%
G3	0.3%	0.4%	0.0%	0.5%	0.7%	-0.3%	0.2%	0.3%	-0.4%	0.6%	0.7%	0.0%
G2	0.0%	0.0%	0.0%	0.0%	0.1%	-0.2%	0.0%	0.1%	-0.4%	0.1%	0.2%	0.0%
G1	–	–	–	–	–	–	–	–	–	–	–	–

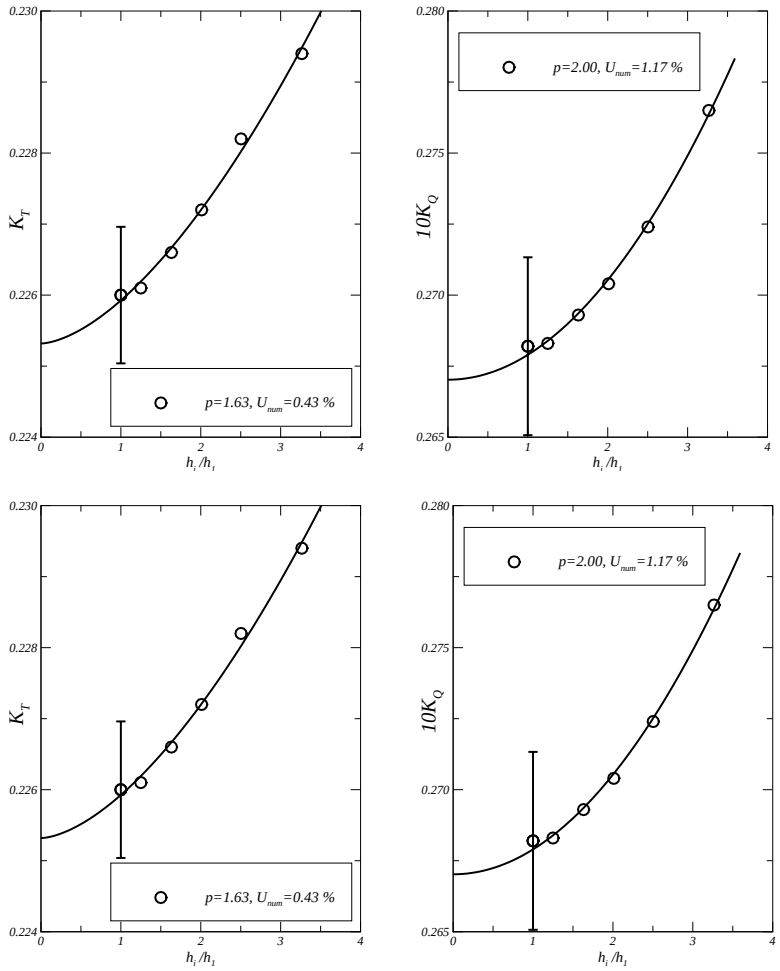

Figure 3: Convergence of the thrust (left) and torque (right) coefficients with the grid refinement ratio h_i/h_1 for propeller S6368 at $J = 0.3$ (top) and for propeller S6408 at $J = 0.2$ (bottom).

Figure 3, where the variation of the thrust and torque coefficients are presented for different grid sizes. Near second-order convergence is obtained for the propeller forces and the numerical uncertainties are in the order of 0.5-1.2%.

Figure 4 presents the limiting streamlines on the suction side for propeller S6408 at $J = 0.2$ calculated with grid G6 and grid G1. From the comparison, different regions of separated flow are obtained near the blade tip. This result shows the importance of the grid density on the calculation of the local flow details. In contrast, the prediction of the propeller forces is less sensitive to the grid density.

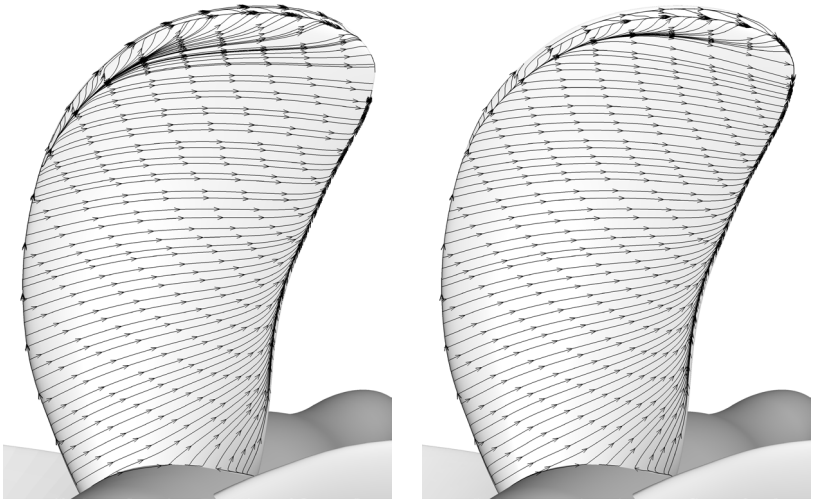

Figure 4: Limiting streamlines on the suction side for propeller S6408 at $J = 0.2$. Comparison between grids G6 (left) and G1 (right).

Table 4: Influence of the domain size for propeller S6408 at $J = 0.2$ and 0.5.

Domain	$J = 0.2$			$J = 0.5$		
Size	K_T	$10K_Q$	η_0	K_T	$10K_Q$	η_0
$3D$	0.2544	0.2915	0.278	0.1284	0.1748	0.585
$5D$	0.2528	0.2902	0.277	0.1278	0.1745	0.583
$10D$	0.2523	0.2889	0.278	0.1276	0.1736	0.585

5.3 Influence of domain size and boundary conditions

First, the influence of the domain size on the performance predictions is presented for propeller S6408. In the previous calculations, the boundaries are placed at $5D$ of the centre of propeller. In this study, the results are compared with domain sizes of $3D$ and $10D$. Grid sizes of 10 million cells and 12.4 million cells were generated for the domain sizes of $3D$ and $10D$, respectively. A fine boundary layer resolution was also applied to obtain y^+ lower than 1. The open-water quantities are compared with the domain size of $5D$ for the 11.3 million grid cells in Table 4. A small effect of the domain size on the force coefficients is seen in the results, since the differences are lower than 1% for all quantities.

Second, the influence of the boundary conditions on the performance predictions is presented. A schematic overview of the computational domain with the boundary definitions is shown in Figure 5. The previous results were obtained, as described previously, assuming a pressure boundary condition for the farfield and a zero normal derivative for the outflow boundary. In this study, a slip-wall is considered for the farfield and a constant pressure at the outflow. An additional case is considered, where an outflow boundary

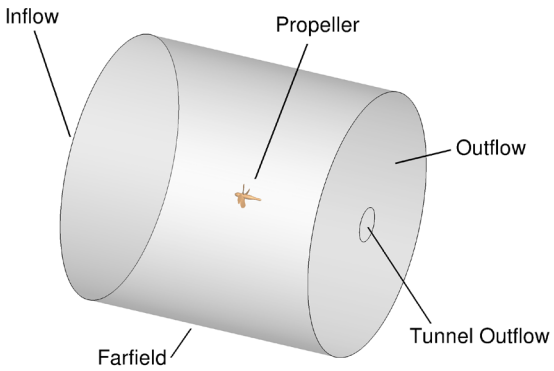

Figure 5: Schematic overview of the domain for the boundary conditions study.

condition is assumed in the centre part of the outflow boundary with a radius of $1.3R$. No changes in the boundary conditions are applied in the inflow boundary and in the propeller and shaft surfaces. The boundary conditions used in this study are listed in Table 5. Table 6 presents the computed force coefficients and open-water efficiency, where a negligible effect of the boundary conditions on the results is seen.

Table 5: Definition of the boundary conditions used for the present calculations.

Boundary Conditions	Boundaries: Inflow	Farfield	Outflow	Tunnel Outflow	Propeller
BC1	uniform vel.	const. pressure	zero normal derivative	zero normal derivative	no-slip wall
BC2	uniform vel.	slip-wall	const. pressure	const. pressure	no-slip wall
BC3	uniform vel.	slip-wall	const. pressure	zero normal derivative	no-slip wall

Table 6: Influence of the boundary conditions on the S6408 propeller forces at $J = 0.2$ and 0.5.

Boundary Conditions	$J = 0.2$			$J = 0.5$		
	K_T	$10K_Q$	η_0	K_T	$10K_Q$	η_0
BC1	0.2528	0.2902	0.277	0.1278	0.1745	0.583
BC2	0.2533	0.2907	0.277	0.1280	0.1747	0.583
BC3	0.2530	0.2902	0.278	0.1277	0.1743	0.583

5.4 Comparison with experimental results

In this section the prediction of the open-water diagram is presented for the two propellers. For the current calculations the grid G3 is used, which reduces significantly the computational effort in comparison with the finest grid. We note that the variation in the force coefficients is lower than 1% between the two grids (Table 3).

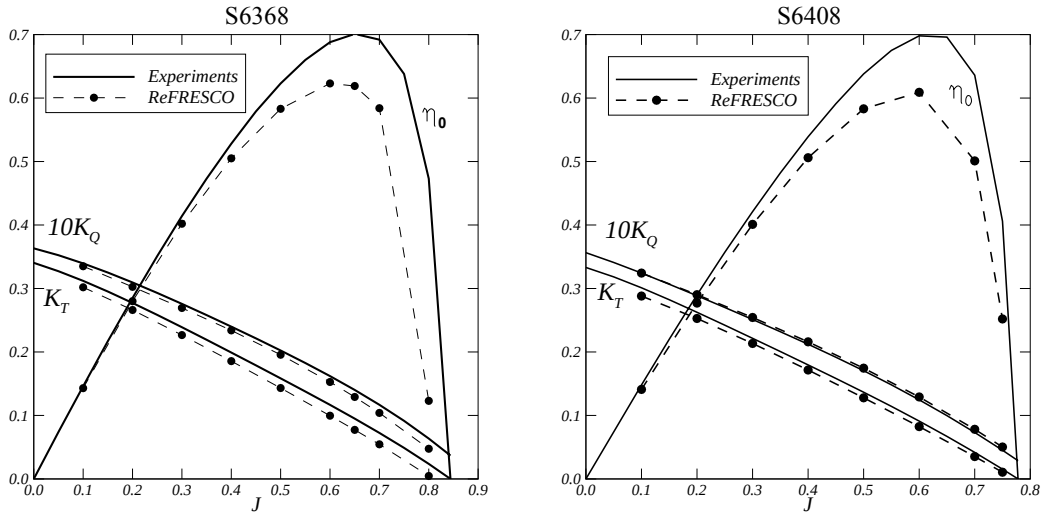

Figure 6: Open-water diagrams for propeller S6368 (left) and propeller S6408 (right).

The comparison between the numerical results and the experimental data available from open-water tests is presented in Figure 6 for both propellers. A large deviation for the high advance coefficients is seen for the S6368 propeller. In this case, the thrust error increases from 3% for $J = 0.1$ to 19% for $J = 0.65$. For the S6408 propeller, smaller differences are found, where the thrust error increases from 4% for low advance ratios to more than 10% for high advance ratios. For both cases, the differences in the propeller torque are in the order of 1% to 3% for advance coefficients up to $J = 0.5$.

Although there is no information about the experimental uncertainties, the relative differences between the numerical and the experimental results (comparison error E) and the numerical uncertainties obtained from the verification study are presented in Table 7. For all cases, the comparison error is larger than the numerical uncertainty, suggesting that the comparison error is dominated by the modelling error. Since the open-water predictions are made in the critical Reynolds number range, different flow regimes, laminar and turbulent may occur simultaneously on the propeller blades. In the calculations the modelling of the laminar-turbulent flow transition is taken care implicitly by the turbulence model.

6 CONCLUSIONS

In this paper, viscous flow calculations using RANS code ReFRESCO are presented for two marine propellers in open-water conditions at model-scale. The influence of the iterative errors, discretisation errors, domain size and boundary conditions on the propeller force predictions has been made. Although large normalised residuals are obtained for the flow quantities, its influence on the forces predictions is assumed to be small due to the fast convergence of the thrust and torque coefficients. The discretisation error has been estimated from a verification study from a range of geometrically similar grids with

Table 7: Comparison between the numerical and the experimental results (comparison error E).

	K_T		K_Q		η_0	
J	E	U_{num}	E	U_{num}	E	U_{num}
	S6368					
0.30	-5.19%	0.43%	-2.36%	1.17%	-2.9%	0.68%
0.65	-18.63%	1.50%	-7.92%	2.17%	-11.7%	0.63%
	S6408					
0.20	-3.70%	2.00%	0.55%	0.31%	-4.5%	0.46%
0.50	-6.44%	1.77%	2.35%	0.73%	-8.6%	0.43%

different densities, where numerical uncertainties in the order of 0.4%-2.2% are obtained for the propeller forces. The influence of the domain size and boundary conditions on the propeller force predictions is found to be smaller than 1%. From the comparison between the numerical and the experimental results, large differences are found suggesting that the comparison error is dominated by the modelling error. It is believed that with the current turbulent model the boundary layer flow at model-scale Reynolds numbers is not correctly captured when both large laminar and turbulent regions are present on the blade. Accordingly, the influence of the turbulence model on the prediction of the open-water diagram at model scale should be considered for future work in order to understand its contribution to the modelling error.

REFERENCES

[1] Eça, L. and Hoekstra, M. A procedure for the estimation of the numerical uncertainty of CFD calculations based on grid refinement studies. *Journal of Computational Physics* (2014) **262**:104–130.

[2] Rijpkema, D. and Vaz, G. *Viscous flow computations on propulsors: verification, validation and scale effects*. In Proceedings of the RINA-Developments in Marine CFD, London, UK, (2011).

[3] Vaz, G., Jaouen, F. and Hoekstra, M. *Free-surface viscous flow computations. Validation of URANS code FRESCO*. In Proceedings of the ASME 28th International Conference on Ocean, Offshore and Arctic Engineering, Honolulu, Hawaii, (2009).

[4] Menter, F. Two-equation eddy viscosity turbulence models for engineering applications. *AIAA Journal* (1994) **32**:1598–1605.

[5] Rijpkema, D., Baltazar, J. and Falcão de Campos, J.A.C. *Viscous flow simulations of propellers in different Reynolds number regimes*. In Proceedings of Fourth International Symposium on Marine Propulsors, Austin, Texas, (2015).